Proceedings of the International Gas Turbine Congress 2003 Tokyo
November 2-7, 2003

IGTC2003Tokyo TS-070

Turbulent Flow Computation in Film-Cooling Turbine Cascades

Boris KURMANOV[1], Masanobu NAMBA[2] and Gregory PODVIDZ[3]

[1]ALSTOM Power Uniturbo, 13 Kasatkin str., Moscow, 129301, Russia
Phone: 7-503-956-6003 ext. 11-64, FAX: 7-503-956-6044,
E-mail: boris.kurmanov@power.alstom.com
[2]Sojo University, Kumamoto, Japan
[3]Central Institute of Aviation Motors, Moscow, Russia

ABSTRACT

A numerical method for investigation of two-dimensional steady, turbulent viscous flow in film-cooling turbine cascade with trailing edge coolant ejection has been developed. Arbitrary number of slots for eject cooling air can be along pressure and suction sides of profile. Navier-Stokes and q-ω turbulence model equations are solved by means of implicit, third-order accuracy in space, monotone Godunov finite volume scheme on O and H type grid. The resulting code is computed considering the mass flow, total temperature and turbulence of injected cooling air in each slot as boundary conditions. The heat transfer results, the pressure distributions and energy loss coefficients have been compared with published experimental data.

NOMENCLATURE

C = velocity magnitude
G = mass flow
J = Jacobian of transformation
k = turbulence kinetic energy
L = chord of profile
Lu = scale of turbulence
M = Mach number
$m = (\rho C)_c / (\rho C)_\infty$ blowing ratio
P = pressure
Q = wall heat flux
q = variable in the q-ω equations, $\sqrt{k}$
Re = Reynolds number
T = temperature
Tu = turbulence intensity
x,y = Cartesian coordinates;
x - normal to cascade plane, y - parallel
α = heat transfer coefficient
β = flow angle, profile design angle
λ = thermal conductivity of the fluid
ε = turbulence energy dissipation
ζ = energy loss coefficient
μ = viscous
ρ = density
ω = variable in the q-ω equations, ε / k

SUBSCRIPTS

1 = inlet
2 = outlet, exit
∞ = free-stream flow
0 (zero) = total (pressure, temperature)
c = coolant
is = isentropic
t = turbulent
te = trailing edge
w = profile

INTRODUCTION

Increasing thermal efficiency of gas turbine engines requires high turbine inlet temperatures. However, the blade material limits this temperature. Film-cooling is used to protect blades exposed to a high-temperature gas flow. The efficiency of film-cooling depends on the distribution of the coolant air over the surface. There are different parameters which affect the film-cooling performance: free-stream turbulence intensity, blowing rate, injection angle, hole geometry and spacing, density ratio, ratio of length scale of cooling air to the hole diameter and others. Taking into consideration the three-dimensionality process (Leylek, 1994; Wilfert, 1996), it is difficult to include all these factors into a single study. At the same time, film-cooling also has an undesirable effect. The injection and following mixing of the cooling air and the main flow lead to changes in the aerodynamic behavior of the blade and in the presence of trailing edge ejection affects especially the flow regime downstream to the cooled blade. Those processes can noticeably decrease the efficiency of the turbine. So, it is very important to select the blowing configuration in such a manner that to avoid negative effects of the coolant ejection on the main turbine parameters, for example on the energy loss coefficient.

Studies of various aspects of film-cooling are widespread in the literature. The most part of them is devoted to the experimental investigation. A detailed turbulence study and aerodynamic description of jets issuing into a crossflow from the inclined hole have been made by Pietrzyk (1989) and Thole (1997). The influence of free-stream turbulence intensity on adiabatic wall cooling effectiveness of the single row film-cooling holes with zero free-stream pressure gradient was investigated by Bons (1996). The comparison of gasdynamic efficiency of two identical stator cascades with coolant ejection through the trailing edge and through the pressure side near the trailing edge was considered by Kapteijn (1996). An investigation of flow field downstream the transonic turbine guide vane annular cascade with 3% and without coolant flow ejection through the slot on the rear pressure side was presented by Sieverding (1996). That test program included wake temperature measurements and wake decay process. It was shown by Arts (1994) the influence of Reynolds and exit Mach numbers, blowing rates on the heat transfer coefficient distribution in film-cooling cascade with eject cooling air in two rows of holes on the pressure and suction sides. The influence of incidence on heat transfer along leading edge and in the immediate vicinity of stagnation point of a film-cooling turbine rotor blade was studied by Camci (1991).

Manuscript Received on March 28, 2003

The number of CFD and analytical studies of film-cooling problem is far less than the experimental one. The dependencies of total pressure loss coefficient as a function of geometric and gasdynamic parameters of cascade with trailing edge coolant ejection have been analytically found by Schobeiri (1989). The important features of jet and crossflow interaction in discrete-jet film cooling were studied by Leylek (1994), comparing the experimental results with 3D Navier-Stokes solution of fully coupled flow in plenum, film-hole, and cross-stream region. Taking as a basis 2D Navier-Stokes solution, it has been demonstrated the influence of injection angle and blowing ratio on film- cooling effectiveness along flat plate (Sarkar, 1996). It was shown by Arts (1994) the comparison of experimental data with heat transfer coefficient computations in 2D guide vane cascade with eject cooling air through two slots on pressure and suction sides of profile.

Many commercial codes designed for study of various external and internal thermo- and gasdynamic applied problems have been appeared in late years (FLUENT, STAR-CD etc.). The ability to solve the tasks with arbitrary real 3D geometry is the main advantage of these codes. At the same time, the majority of commercial codes is based on the finite-difference schemes of the second-order approximation in space, that is not quite enough on nonstructural grids for resolve of thin flow structure. The programs created for the solution of any specific task appear frequently to be more exact and effective.

The basic objective of the given work was the development of the fast 2D Navier-Stokes code to the predicted film-cooling and trailing edge ejection in turbine cascade for parametric runs in preliminary design-type settings instead of the two-dimensional boundary layer code.

MATHEMATICAL MODEL

The Reynolds-averaged Navier-Stokes equations are used to obtain the computational results presented in this paper. The turbulent viscosity coefficient μ_t is calculated using the two-equations (q-ω) low Reynolds number model of turbulence proposed by Coakley (1983). In this model the quantities q and ω are related with the kinetic energy of turbulence k and the dissipation ratio ε as: $q = k^{1/2}$, $\omega = \varepsilon / k$. The chosen turbulent model has the better numerical behavior compared to the k - ε model. This can be seen if one compares the source terms for ε and ω equations. In view of the boundary condition on the profile is k = 0 the source term in ε equation of the turbulence model contains the singularity k^{-1} type, while the ω equation is free from this shortcoming. The full system of two-dimensional, unsteady equations is written in curvilinear body-fitted coordinates $\xi=\xi(x,y)$ - along normal to profile, $\eta=\eta(x,y)$ - along profile (Fig.1) and has the following conservation form:

$$\frac{\partial \mathbf{U}}{\partial t} + \frac{\partial \mathbf{E}}{\partial \xi} + \frac{\partial \mathbf{F}}{\partial \eta} = \frac{\partial \mathbf{R}}{\partial \xi} + \frac{\partial \mathbf{S}}{\partial \eta} + \mathbf{Q} \qquad (1)$$

where:

$$\mathbf{U} = J^{-1}\begin{pmatrix} \rho \\ \rho u \\ \rho v \\ E \\ \rho q \\ \rho \omega \end{pmatrix}, \quad \mathbf{E} = J^{-1}\begin{pmatrix} \rho U \\ \rho u U + P\xi_x \\ \rho v U + P\xi_y \\ (E+P)U \\ \rho q U \\ \rho \omega U \end{pmatrix}, \quad \mathbf{F} = J^{-1}\begin{pmatrix} \rho V \\ \rho u V + P\eta_x \\ \rho v V + P\eta_y \\ (E+P)V \\ \rho q V \\ \rho \omega V \end{pmatrix}.$$

The contravariant velocity components are written as

$$U = \xi_x u + \xi_y v, \qquad V = \eta_x u + \eta_y v \qquad (2)$$

and the viscous flux terms are assembled in the form

$$\mathbf{R} = J^{-1}\begin{pmatrix} 0 \\ \xi_x \tau_{xx} + \xi_y \tau_{xy} \\ \xi_x \tau_{yx} + \xi_y \tau_{yy} \\ \xi_x \beta_x + \xi_y \beta_y \\ (\mu + \mu_t/\sigma_q)(\xi_x q_x + \xi_y q_y) \\ (\mu + \mu_t/\sigma_\omega)(\xi_x \omega_x + \xi_y \omega_y) \end{pmatrix},$$

$$\mathbf{S} = J^{-1}\begin{pmatrix} 0 \\ \eta_x \tau_{xx} + \eta_y \tau_{xy} \\ \eta_x \tau_{yx} + \eta_y \tau_{yy} \\ \eta_x \beta_x + \eta_y \beta_y \\ (\mu + \mu_t/\sigma_q)(\eta_x q_x + \eta_y q_y) \\ (\mu + \mu_t/\sigma_\omega)(\eta_x \omega_x + \eta_y \omega_y) \end{pmatrix}, \qquad (3)$$

where the shear stresses are related to the strains by the following relationships:

$$\begin{aligned} \tau_{xx} &= \mu_\Sigma\left[\frac{4}{3}(\xi_x u_\xi + \eta_x u_\eta) - \frac{2}{3}(\xi_y v_\xi + \eta_y v_\eta)\right], \\ \tau_{yy} &= \mu_\Sigma\left[\frac{4}{3}(\xi_y v_\xi + \eta_y v_\eta) - \frac{2}{3}(\xi_x u_\xi + \eta_x u_\eta)\right], \\ \tau_{xy} &= \tau_{yx} = \mu_\Sigma(\xi_y u_\xi + \eta_y u_\eta + \xi_x v_\xi + \eta_x v_\eta), \\ \beta_x &= u\tau_{xx} + v\tau_{xy} + \overline{\mu}_\Sigma i_x, \\ \beta_y &= u\tau_{yx} + v\tau_{yy} + \overline{\mu}_\Sigma i_y, \qquad \overline{\mu}_\Sigma = \mu/\mathrm{Pr} + \mu_t/\mathrm{Pr}_t. \end{aligned} \qquad (4)$$

The source terms of the turbulence model are

$$\mathbf{Q} = J^{-1}\begin{pmatrix} 0 \\ 0 \\ 0 \\ 0 \\ 0.5(C_\nu f_1 D/\omega^2 - 1)\rho q \omega \\ (C_1 C_\nu D/\omega^2 - C_2)\rho \omega^2 \end{pmatrix} \qquad (5)$$

in which

$f_1 = 1.0 - \exp(-\alpha\, \mathrm{Re}_n)$, $C_1 = 0.405 f_1 + 0.045$,

where the term $\mathrm{Re}_n = \rho q n/\mu$ is the turbulence Reynolds number based on the distance from the wall (n) and

$$D = 2[(u_\xi \xi_x + u_\eta \eta_x)^2 + (v_\xi \xi_y + v_\eta \eta_y)^2] + (u_\xi \xi_y + u_\eta \eta_y + v_\xi \xi_x + v_\eta \eta_x)^2 \qquad (6)$$

is the rate of production of turbulent kinetic energy. In the above, α = 0.0065, σ_q = 1, σ_ω = 1.3, Pr = 0.71, Pr_t = 0.9, C_2 = 0.92, C_ν = 0.09 . The turbulent viscosity is defined as:

$$\mu_t = C_\nu f_1 \rho \frac{q^2}{\omega}, \qquad (7)$$

and the laminar viscosity is modeled by Sutherland's law in which μ is a function of the local static temperature. The laminar/turbulent transitions are not specified in q-ω turbulent model and are triggered by the numerical procedure.

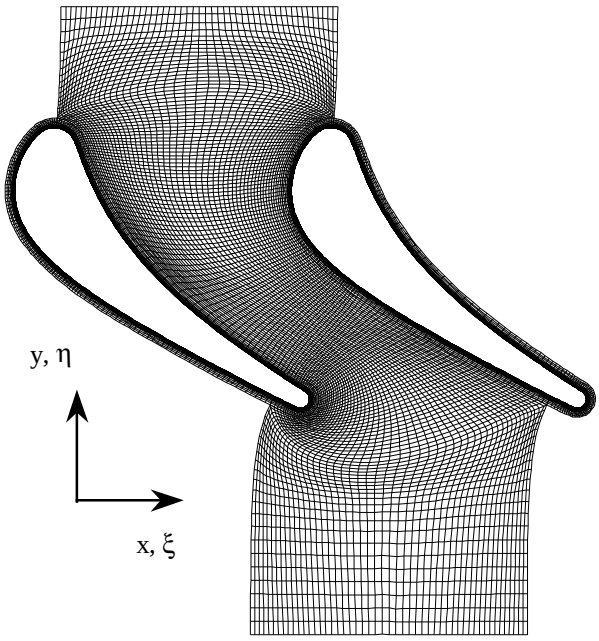

Fig.1 Computational O and H type grid system

The systems of Navier-Stokes and turbulence equations are advanced in time using an implicit, third-order accuracy in space, finite-difference scheme proposed by Godunov (Godunov, 1976; Krupa, 1994; Kurmanov, 1999). Here, the method has been modified for cascades with eject cooling air through slots on pressure and suction sides of profile. The numerical procedure consists of the following:

- The finite-difference Navier-Stokes and q-ω systems equations are solved separately one after another in matrix form.
- Using the Beam and Warming (1978) time digitization each system of equations is written in implicit, unfactored finite difference delta form for computation cell i,j :

$$\left[\mathrm{I}+\theta\tau J\left(\nabla_\xi \mathrm{A}^+ + \Delta_\xi \mathrm{A}^- + \nabla_\eta \mathrm{B}^+ + \Delta_\eta \mathrm{B}^- - \nabla_\xi \Delta_\xi \mathrm{M} - \nabla_\eta \Delta_\eta \mathrm{N} - \mathrm{W}\right)\right]^n_{i,j} \cdot \delta \mathbf{U}^{n+1}_{i,j} =$$

$$= -\tau J\left(\mathbf{E}_{i+\frac{1}{2},j} - \mathbf{E}_{i-\frac{1}{2},j} + \mathbf{F}_{i,j+\frac{1}{2}} - \mathbf{F}_{i,j-\frac{1}{2}} - \mathbf{R}_{i+\frac{1}{2},j} + \mathbf{R}_{i-\frac{1}{2},j} - \mathbf{S}_{i,j+\frac{1}{2}} + \mathbf{S}_{i,j-\frac{1}{2}} - \mathbf{Q}_{i,j}\right)^n,$$

where **E**, **F** are the inviscid and **R**, **S** are the viscous fluxes through cell boundaries in ξ,η directions. The Jacobi matrices A^+, A^- along ξ and B^+, B^- along η directions have either positive or negative eigenvalues and are expressed as $A = \partial \mathbf{E} / \partial \mathbf{U} = A^+ + A^- = S_\xi \Lambda^+_A S^{-1}_\xi + S_\xi \Lambda^-_A S^{-1}_\xi$, $B = \partial \mathbf{F} / \partial \mathbf{U} = B^+ + B^- = S_\eta \Lambda^+_B S^{-1}_\eta + S_\eta \Lambda^-_B S^{-1}_\eta$. Here, Λ_A, Λ_B are diagonal matrices composed of eigenvalues of matrices A , B and S_ξ, S_η are transformation matrices. The matrices M, N, W are defined as $M = \partial \mathbf{R} / \partial \mathbf{U}$, $N = \partial \mathbf{S} / \partial \mathbf{U}$, $W = \partial \mathbf{Q} / \partial \mathbf{U}$. Superscript n refers to the instant of time $t = n\tau$, two integer subscripts refer to the value of the functions at the center of computational cell, while integer and half-integer refer to the value of the function at a cell boundary. We let $\delta \mathbf{U}^{n+1}_{i,j} = \mathbf{U}^{n+1}_{i,j} - \mathbf{U}^n_{i,j}$. Symbols ∇_ξ ,∇_η and Δ_ξ, Δ_η are the first-order backward and forward difference operators along ξ and η directions, ∇Δ is the second-order center difference operator. The splitting of the Jacobi matrices and the use of upwinding differences (in accordance with the sign of eigenvalues) enable one to increase the stability of the finite-difference scheme.

- The inviscid fluxes in the right side of finite-difference equations along ξ,η directions are calculated using piecewise parabolic parameters distributions for characteristic variables ($\delta \mathbf{W}_\xi = S^{-1}_\xi \delta \mathbf{U}$, $\delta \mathbf{W}_\eta = S^{-1}_\eta \delta \mathbf{U}$) into cells, condition of monotonicity and procedure for solving the problem of the breakdown of an arbitrary discontinuity (exact solution of Riemann problem at cells boundary). In viscous fluxes the partial derivatives are approximated by central differences the second-order accuracy.

The implicit operator in the left side of finite-difference equations is inverted using iterative Gauss-Seidel method along lines η=const. At every time step two "internal" iterations are fulfilled. All boundary conditions in implicit operator are realized an implicit manner. It allows to carry out calculations with Courant number down to 50.

- Because only a steady result is desired, local time stepping is used.

The method does not require the introduction of terms with artificial dissipation and makes it possible to obtain stable solution with the third-order accuracy in space on uniform grid.

GRID AND BOUNDARY CONDITIONS

A high-quality computational grid is necessary to ensure the success of the numerical computations. The combined O- and H-grid has been chosen at presented analysis. On the first stage, inside every slot on pressure and suction sides of profile the H-grid is generated by algebraic method with condense near the walls. The O-grid around profile is also built in algebraic manner, considering the slot's grid nodes lying on pressure and suction sides of profile. The O-grid has rectangular cells with orthogonal to profile edges and can be easily stretched and compressed along the both tangential ξ and normal η to profile directions. In the immediate vicinity of the wall three rows of cells with thickness about 10^{-5} L are located. At that rate the wall Y^+ values are inside the range $Y^+<0.4$ for typical turbine cascades. On the second stage, the H-grid is generated by solving the second-order elliptic system of differential equations (Godunov, 1976), using the O-grid nodes location. Before and behind cascade the H-grid has periodic nodes. Figure 1 shows the form of O- and H- grid system, obtained by this method. The grid for guide vane cascade without slots has about 1700 number of cells. The basic advantages of such a grid are smooth variation of the size and the shape of cells as well as their nearly orthogonal form. There are the most skew cells behind trailing edge at H- grid. Nevertheless, the real order of accuracy of finite-differences scheme on such cells is between the second and the third. In Fig.2 there is shown a zoomed view of the real computation grid near and inside slots on the pressure side of profile.

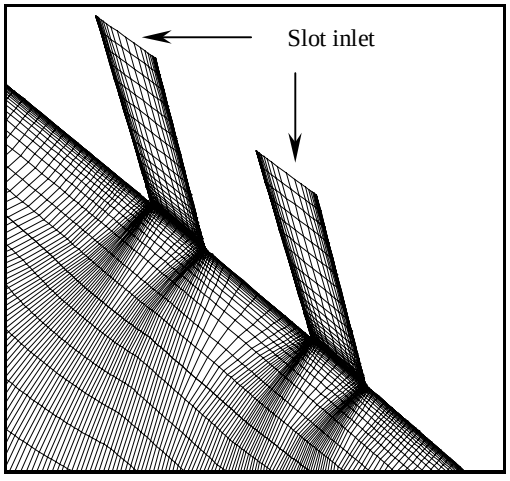

Fig.2 Grid shape near the slots

There are five different types of boundary in film-cooling cascade: inlet, outlet, solid wall, periodicity and inlets inside slots.

For subsonic-axial velocity the flow angle, total pressure, total temperature, intensity and length scale of turbulence are imposed on the inlet boundary.

$$\beta_1,\ P_{01},\ T_{01},\ Tu_1,\ Lu_1 .$$

The inlet length scale is usually not reported as a part of the experimental conditions. At the same time, this parameter (together with intensity of turbulence) defines the quantity of inlet gas turbulent viscosity and influences, for example, on overall level of total pressure losses. For cascade conditions the dissipation length scale is assumed to be equal to a certain percent of the profile chord length. The assumption $Lu_1 = 2\%$ was made in the course of the calculations performed in this work. The inlet turbulence variables q_1 , ω_1 are defined through intensity, length scale of turbulence and inlet cascade velocity C_1 as follows:

$$q_1 = \sqrt{1.5}\ Tu_1\, C_1 , \qquad \omega_1 = q_1 / Lu_1 \quad .$$

The inlet boundary inside slot is treated just as inlet cascade boundary with uniform cooling air parameters, so the total temperature, flow angle, coolant mass flow and turbulence parameters are specified. The total pressure of coolant is obtained as computation result. On the other boundaries the typical cascade boundary conditions are imposed.

The improved points of the method are: taking into consideration the eject of cooling air on a profile, using the completely implicit boundary conditions and third order accuracy in space, using the regular quasi-orthogonal grid in whole computational domain.

CASCADE WITH TRAILING EDGE AIR EJECTION

Transonic turbine guide vane cascade with coolant ejection through trailing edge was selected for comparison of the advanced numerical method with experimental data obtained by Kapteijn (1996) at al. The shape of cascade and most important geometric characteristics are presented in Fig.3. All numerical results without and with 3% coolant ejection were obtained for inlet flow parameters: P_{01}=1.0bar, T_{01}=300K, β_1=90°, Tu_1=0.45% which corresponds to the conditions of experiment. The blade temperature was T_w=300K and Reynolds number, based on chord length and design outlet velocity, made approximately $Re=10^6$. The downstream isentropic Mach number was changed in a range $0.65 \le M_{2,is} \le 1.25$ with increment 0.1 , where the design Mach number $M_{2,is}$=1.05 was included.

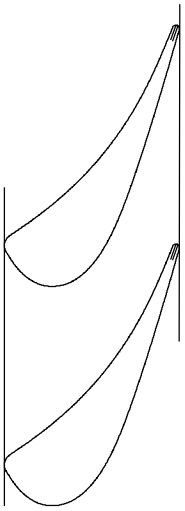

Chord length L = 72.0 mm
Axial chord length
b = 43.24 mm
Pitch-to-chord ratio
t/L = 0.7523
Throat width a =14.97mm
Stagger angle γ = 38.1°
Trailing edge thickness
d_{te} = 1.7 mm
Trailing edge wedge angle
ω_{te} = 6.4°
Slot width sl = 0.55 mm
Inlet design angle
β = 90.0°

Fig.3 Cascade geometry

Because of only gasdynamic, aspects of the trailing edge blowing out were experimentally studied, the total temperature of the coolant air was adjusted exactly to the total temperature of the main flow $T_{0C}=T_{01}$. The computational O and H type grid in cascade contained 24700 of total number of cells, including 1300 cells inside slot. The experimental and computational isentropic Mach number distributions over the profile at $M_{2,is}$ =1.05 both 3% coolant ejection and 0% are shown in Fig.4. The predicted and experimental positions of the maximum of velocity on the suction side coincide well. This maximum of velocity is a result of incident shock wave propagates from trailing edge of the neighboring profile. The greatest discrepancy of results is observed on the rear part of the almost linear suction side in transonic range of velocity, where the flow is very sensitive to variation of profile shape.

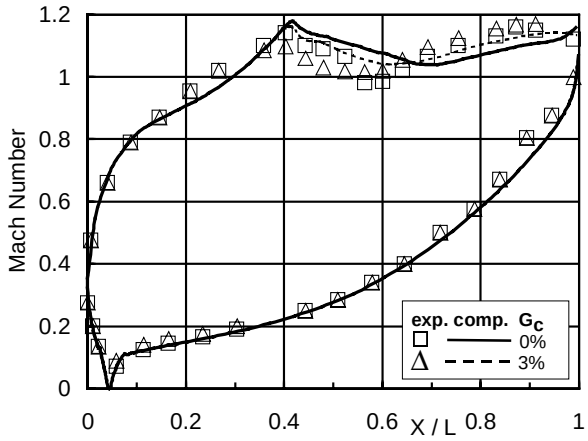

Fig.4 Mach number distribution over the profile at $M_{2,is}$=1.05

Along pressure side the computed results are in considerably good agreement with the experiment. According to experimental data on a site, $0.4<x/L<0.55$ is a thin separation bubble as a result of strong interaction oblique shock wave with boundary layer on the suction side. Figure 5 shows the computed skin friction coefficient along the suction side with and without coolant ejection. The site with negative skin friction coefficient is present in both cases in a place of the positive pressure gradient. That indicates the separate nature of flow in the vicinity of interaction oblique shock wave with boundary layer on suction side. The separation bubble decreases in case with ejection for this cascade and flow parameters.

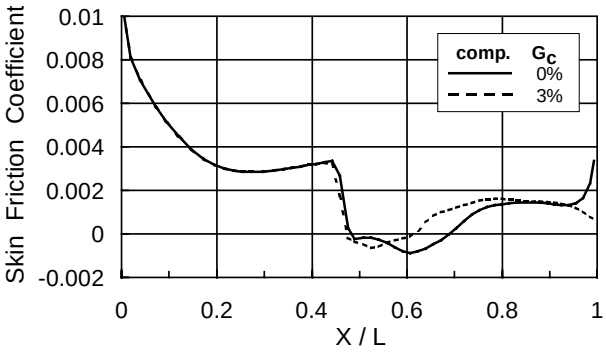

Fig.5 Skin friction coefficient over suction side of profile

It should be noted the predicted length of separation bubble ($x/L \approx 0.15$) for flow with 3% ejection is exactly coincident with experimental one. Calculations have shown that effect of coolant ejection is rather small, reducing the local maximum and insignificant redistribute Mach number on the suction side.

The base pressure coefficient as a function of downstream isentropic Mach number is shown in Fig.6 and defined as:

$$\Delta P_{te} = \frac{P_{te} - P_2}{0.5\rho_{2,is} C_{2,is}^2}, \qquad (8)$$

where P_{te} is the average pressure in separation zone behind the trailing edge. The predicted and experimental values of ΔP_{te} without ejection are negative (excepting the point M_2=1.0 where the experimental value is near zero) and has the same quality Mach number dependence, but calculations of some underpredicted values of ΔP_{te} within all range of $M_{2,is}$ are made for this cascade. The coolant ejection increases the base pressure and shifts up the curve.

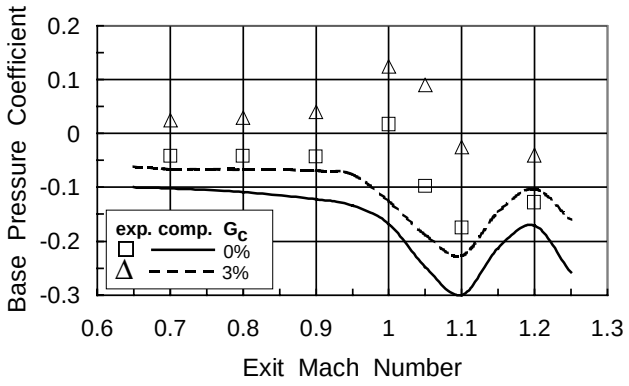

Fig.6 Base pressure coefficient

The small discrepancy between experimental and computation absolute values of ΔP_{te} can explain the difference of manner of measurement and calculation. As it is known, in case with ejection, the base pressure coefficients behind pressure and suction sides of trailing edge are different. Here, this function has been calculated as average in both separation zones. On the other hand, the author of the experiment (Kapteijn at al., 1996) has written: "The pressure tap for measuring the base pressure ΔP_{te} on the trailing edge ejection blade is positioned in one of the struts in the coolant ejection slot". But the pressure inside slot is higher than in separation zones and, therefore, the experimental base pressure coefficient should be higher than the predicted one.

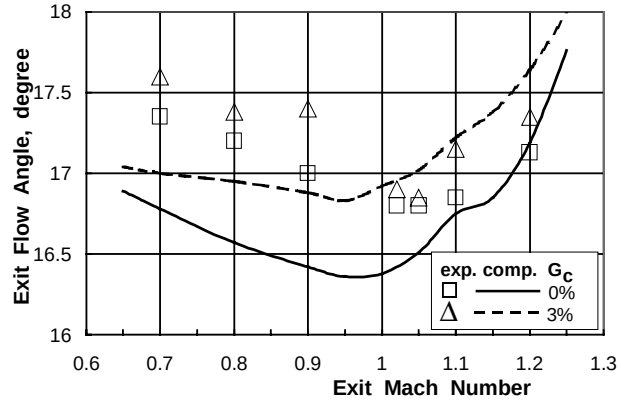

Fig.7 Exit flow angle

Comparison of the outlet flow angle (Fig.7) gives a good agreement. The maximum discrepancy ≈ 0.6° is observed in subsonic range of $M_{2,is}$ and corresponds to the real measurement accuracy of flow angle. In accordance with the Fig. 7, the turn of the flow measured in the experiment reaches maximum near $M_{2,is}$ = 1.03, while the computations indicate the position nearly $M_{2,is}$ ≈ 0.96. The ejection of 3% cooling air through trailing edge a little bit changes the exit flow angle.

The energy loss coefficient ζ is based on the energy difference across the cascade. Usually for film-cooling cascade the losses ζ is calculated taking into account the energy input as a result of the coolant ejection:

$$\zeta = 1 - \frac{1 + \sum \overline{G}}{1 + \sum \overline{G} \cdot \overline{H}} \varphi^2, \quad \varphi = C_2 / C_{2,is}, \quad \overline{G} = G_c / G_1,$$

$$\overline{H} = \frac{T_{0c}}{T_{01}} \left[1 - \left(\frac{P_2}{P_{0c}} \right)^{\frac{k-1}{k}} \right] \Bigg/ \left[1 - \left(\frac{P_2}{P_{01}} \right)^{\frac{k-1}{k}} \right], \qquad (9)$$

where $\sum$ - is a summation by all slots. Figure 8 shows the energy loss coefficient as a function of downstream isentropic Mach number with the coolant as a parameter. The experimental data are shown without taking into accounts the energy input as a result of the coolant ejection ($\overline{G}, \overline{H} = 0$). The predicted results without ejection are in a good agreement with experimental data.

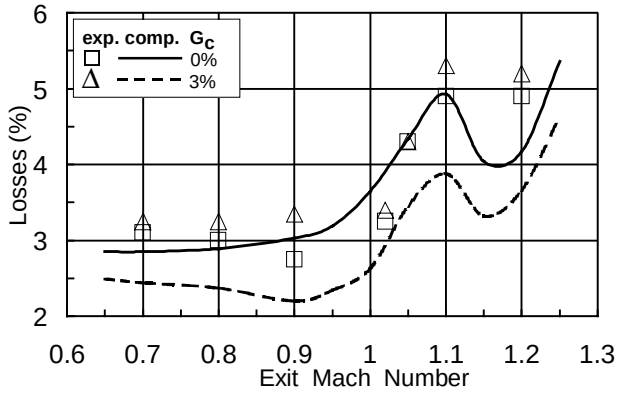

Fig.8 Energy loss coefficient

For subsonic exit Mach number ($M_{2,is} \leq 0.95$) the ζ is almost constant, then sharply increases. The losses measured for case with 3% air ejection are practically the same or slightly higher in comparison with the case G_C=0. The small air ejection G_C =1÷3% changes the velocity distribution over profile (and skin friction coefficient), decreases the total pressure and velocity gradients in near wake (and mixing losses), introduces the additional energy and mass into flow. As a result, for subsonic outlet velocity $M_{2,is}$ the coolant ejection decreases the losses in most cases (Venediktov et al., 1990). For transonic and supersonic outlet velocity $M_{2,is}$ the effect of coolant ejection is ambiguously. Under the influence of ejection the wake makes thicker, the trailing edge shock waves move upstream and locate in the immediate vicinity of the trailing edge and velocity field is deformed. It can result both to decrease and to growth of the losses. At present case the predicted results indicate the decrease losses in all range of $M_{2,is}$ number. It is necessary to note the nonmonotonic behavior of computation losses in a range $1.05 < M_{2,is} < 1.25$. Similar dependencies $\zeta(M_2)$ take very often place in cascade, but the experimental point at $M_{2,is}$ =1.15 isn't available in present research. Obtained in the experiment difference of base pressure coefficient (Fig.6) at a design point $M_{2,is}$ = 1.05 with/without ejection is rather large $\Delta P \approx 0.2$. In this case the losses difference should be also appreciable, however, losses are identical.

The predicted and measured total pressure ratio, static/total pressure ratio and flow angle across the wake at the axial distance of 0.486L behind cascade with 3% air ejection at $M_{2,is}$ =1.05 are shown in Fig.9. The best coincidence is observed for total pressure

distribution. The maximum discrepancy of experimental and computational flow angle is about ≈0.9° that is close to real measurement accuracy. The predicted distribution of static pressure shows growth of pressure in a compression wave extending from a trailing edge of profile. Calculations have also shown the small flow angle variation under the flow passage through an oblique shock wave. The Mach number contours for design point $M_{2,is}$ =1.05 and 3% air ejection is shown in Fig.10.

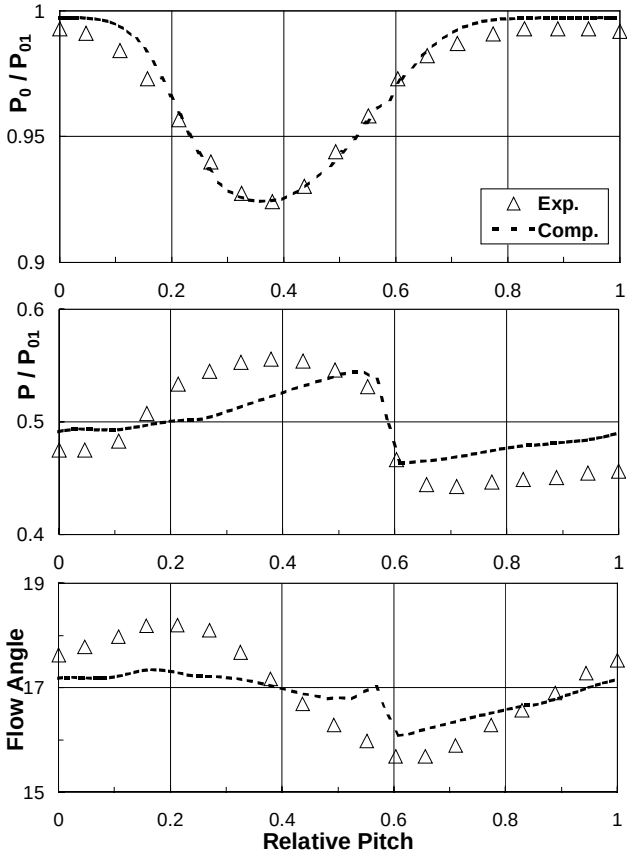

Fig.9 Flow parameters distribution: P_0/P_{01}, P/P_{01}, flow angle across the wake with 3% air ejection at $M_{2,is}$=1.05

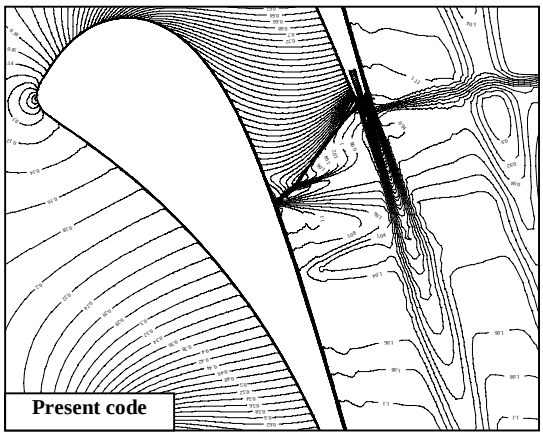

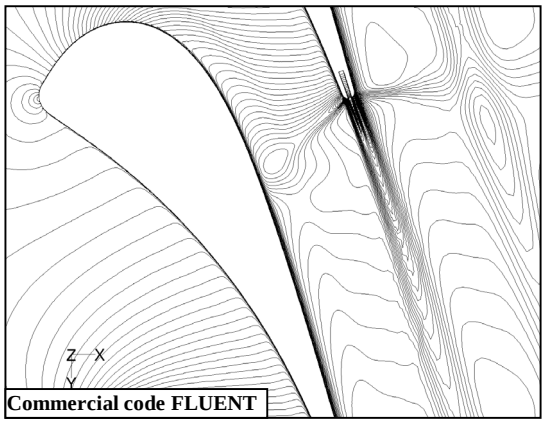

Fig.10 The Mach number contours at $M_{2,is}$=1.05

The shock system associated with the trailing edge is clearly resolved on the top part of figure. On the bottom part is shown the result obtained on a similar grid with the help of commercial software FLUENT which has a second order approximation in a space. In this case the trailing edge shock is strongly smeared and does not cause separation of a boundary layer on suction side.

FILM-COOLING CASCADE

A transonic turbine guide vane cascade with pressure and suction sides coolant ejection was aero-thermal experimentally investigated by Arts (1994). The shape of cascade with position of two rows of the holes on pressure and suction sides and most important geometric characteristics are shown in Fig.11.

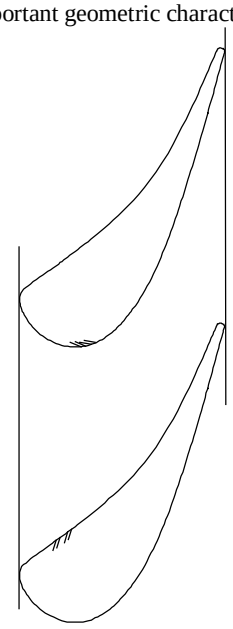

Chord length L = 67.94 mm
Axial chord length
b = 36.31 mm
Pitch-to-chord ratio
t/L = 0.8463
Throat width a = 14.93mm
Stagger angle γ = 34.37°
Trailing edge thickness
d_{te} = 1.45mm
Trailing edge wedge angle
ω_{te} = 7°
Hole diameter = 0.5mm
Inlet design angle β = 82.0°

Fig.11 Cascade geometry

The numerical results with pressure and suction sides coolant ejection were obtained for the following inlet flow parameters: T_{01}=402K, β_1=90°, Tu_1=1.0%, 6.0% which correspond to the conditions of experiment. The inlet total pressure was changed from 0.83 up to 3.3bar in order to simulate the Reynolds number in diapason Re =$0.5\times10^6 \div 2\times10^6$. The profile temperature was T_w=302K. The heat transfer coefficient α for film-cooling cascade was defined as:

$$\alpha = \frac{Q_w}{T_{aw} - T_w}$$

where T_{aw} - adiabatic wall (profile) temperature. In practice it was calculated in two stages. The flow with eject cooling air and

adiabatic wall boundary condition $(\partial T/\partial n)_w = 0$ is computed on the first stage. In a result, there is a local adiabatic profile temperature T_{aw} (film temperature). On the second stage, the flow with ejects cooling air and prescribed wall temperature T_w is computed. In a result, the local heat fluxes on the profile Q_w and heat transfer coefficient α are obtained.

Calculations have been made for ejection cooling air through two slots on suction side of profile for different exit Mach number and blowing ratio. Figure 12 compares the predicted and measured heat transfer coefficient distribution for m =0.29, 0.71 with $M_{2,is}$ = 0.7; Re = 10^6 and Tu_1 = 1.0%. On the suction side of profile for low blowing ratio m = 0.29 the prediction is quite good, but for larger ratio m =0.71 in the immediate vicinity behind the slots calculation showed reduced value of heat transfer coefficient. On the rear part of suction side the predicted results nearly match the experimental one.

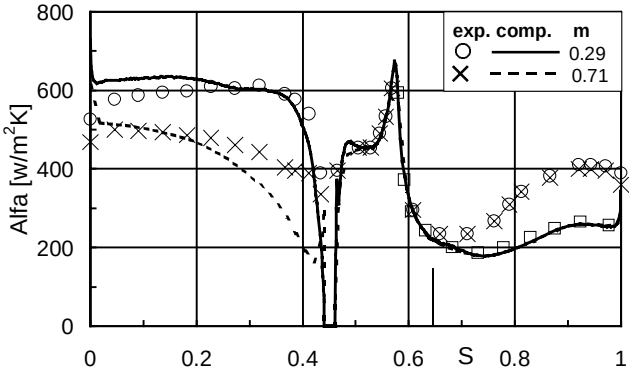

Fig.12 Profile heat transfer distributions: $M_{2,is}$=0.7, Re = 10^6 , Tu_1 = 1%

Along pressure side for both blowing ratio the predictions are extremely good only before position S ≈0.64 (marked vertical line) where the blowing slots are located. Behind slots the computational results correspond to the development of a laminar boundary layer. At the same time the experimental heat transfer coefficient indicates that the transition is triggered just near the slots. The most probable reason of this is that the real blowing slots in the experimental profile play a role of the generator of turbulence (even without ejection) but its influence isn't taken into consideration in numerical procedure. In order to confirm that supposition, in Fig.12 there are shown the experimental data (quadrates) obtained by Arts (1992) on smooth profile (without slots) under the same conditions of experiments. These results are extremely well correspondent with present computations.

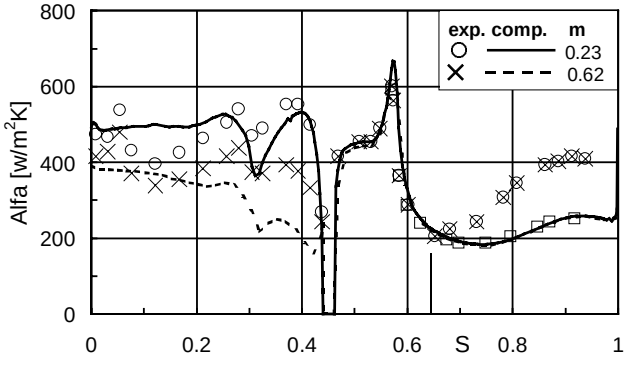

Fig.13 Profile heat transfer distributions: $M_{2,is}$=1.1, Re = 10^6 , Tu_1 = 1%

For Mach number $M_{2,is}$ =1.1 the comparison has been made for two blowing ratio m =0.23, 0.62 with Re =10^6 and Tu_1 =1.0% (Fig.13). The behavior heat transfer coefficient along pressure side is similarly the previous case for $M_{2,is}$ =0.9. The quadrates in Fig.13 indicate the experimental data obtained for smooth profile without slots. The heat transfer coefficient has non-monotone character on the suction side of profile behind the blowing slots. For the lowest blowing ratio m=0.23 the calculated results match nearly the measured data, excepting the vicinity S≈0.12. For blowing ratio m=0.62 the predicted results starting from a position at once behind the slots and up to a position S≈0.22 appreciably lower experimental data. Near the trailing edge on the rear part of the suction side the comparison is satisfactorily enough. The local minimum of heat transfer near the position S≈0.31 is caused by incident shock wave propagates from the trailing edge of nearest profile. Computed iso-Mach number lines inside and near the slots on the suction side of profile are presented in Fig.14. The separation zones between slots and behind second slot are clearly observed.

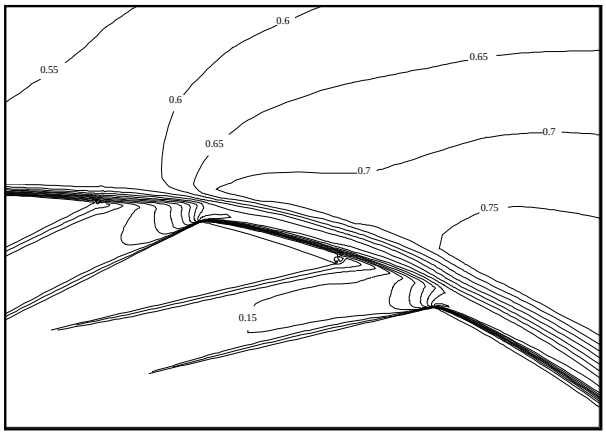

Fig. 14 The Mach number contours near the slots

Calculations have also been made for ejection cooling air from two slots on pressure side of profile for different flow parameters. The Figure 15 compares the predicted and measured heat transfer coefficient distribution for blowing ratio m =2.04 and following flow parameters: $M_{2,is}$ =0.9 , Re =2×10^6 , Tu_1 =1.0%. Beginning from the leading edge stagnation point to slots on the pressure side the computed results are exactly coincident with experiment, but immediately behind the holes on the interval 0.66<S<0.82 the heat transfer is underpredicted and overpredicted on the rear part of pressure side.

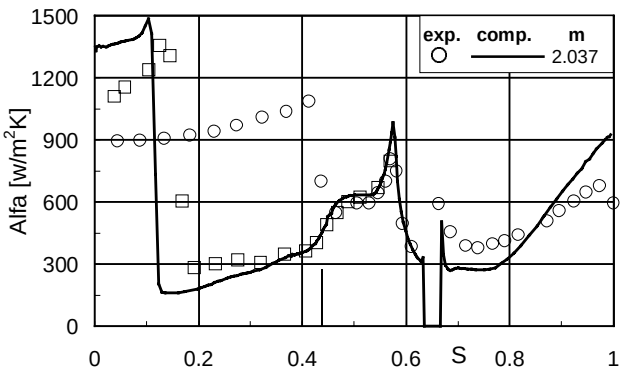

Fig.15 Profile heat transfer distributions: $M_{2,is}$=0.9, Re =2×10^6, Tu_1 = 1%

Beginning from the leading edge along the suction side the prediction is extremely good only to position S≈0.45 (marked vertical line) where the blowing slots (without ejecting) are located. Behind the slots the computational results correspond to the experimental data obtained on smooth profile (quadrates). Figure 15 shows that position of the transition onset on the suction side as well as on the pressure side in the previous case coincides with the slots location (S≈0.45).

The predicted and experimental heat transfer coefficient distributions for large blowing rate on the pressure side m =3.03, high inlet turbulence intensity Tu_1 =6.0%, low Reynolds number Re = 0.5×10^6 and $M_{2,is}$ =0.9 are shown in Fig.16. As it was expected, the general level of heating is lower in comparison with previous case for higher Reynolds number. On the pressure side a good enough conformity is observed on the leading edge and on the middle part of profile. At once behind the slots and on the rear part of pressure side the experimental data exceed the computed heat transfer coefficient. It should take notice of extremely high experimental value α≈455 near the edge of the slot S≈0.66.

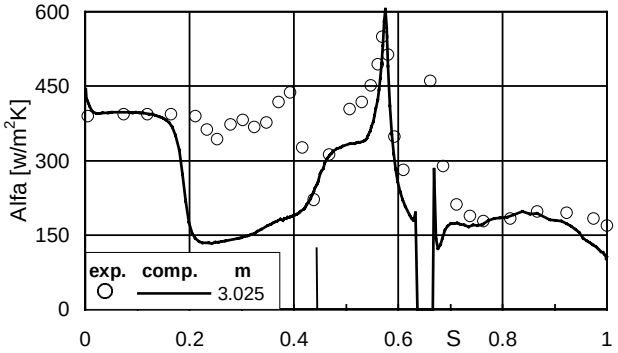

Fig.16 Profile heat transfer distributions: $M_{2,is}$=0.9, Re =0.5×10^6, Tu_1 = 6%

On the suction side the experimental position of the transition onset is observed at once behind the slots (vertical line). The predicted boundary layer transition starts on the rear part of profile and heat transfer coefficient reaches the same value as experimental one. The comparison with experimental data has shown that slots have an influence on behavior of boundary layer and their presence should be taken into consideration somehow in computations.

CONCLUSIONS

An unfactored implicit third-order accuracy finite difference method has been developed for the numerical solution of two-dimensional Navier-Stokes equations with *q*-ω model of turbulence in order to predict the gasdynamic and thermal features of flow in film-cooling gas turbine cascade.

For guide vane cascade with trailing edge air ejection the predicted losses, exit flow angle and velocity distribution quite well coincide with experimental data. Calculations have shown that 3% air ejection through trailing edge decreases energy loss coefficient and slightly modifies pressure distribution on rear part of suction side.

For cascade with ejects cooling air on suction or pressure sides of profile the present method showed a quality and in some cases a quantity agreement with experimental film-cooling heat transfer coefficient. A comprehensive investigation is required to determine the influence kinetic energy and length scale turbulence of coolant on film-cooling performances.

REFERENCES

Ameri, A.A., Sockol, P.M., Gorla, R.S.R., 1992, "Navier-Stokes Analysis of Turbomachinery Blade External Heat Transfer", *Journal of Propulsion and Power*, **8**, No. 2, pp. 374-381.

Arts, T., 1994, "Test Case No2: Highly Loaded Transonic and Film Cooled Liner Turbine Guide Vane Cascade LS94", Numerical Methods for Flow Calculation in Turbomachines, VKI Lecture Series 1994-06.

Arts, T., Lambert de Rouvroit, M., 1992, "Aero-Thermal Performance of a Two-Dimensional Highly Loaded Transonic Turbine Nozzle Guide Vane: A Test Case for Inviscid and Viscous Flow Computations", ASME *Journal of Turbomachinery*, **114**, pp.147-154.

Beam, R.M., and Warming, R.F., 1978, "An Implicit Factored Scheme for the Compressible Navier-Stokes Equations", AIAA *Journal*, **16**, pp. 393-401.

Bons, J.P., MacArthur, C.D., and Rivir, R.B., 1996, "The Effect of High Free-Stream Turbulence on Film Cooling Effectiveness", ASME *Journal of Turbomachinery*, **118**, pp. 814-825.

Camci, C., and Arts, A., 1991, "Effect of Incidence on Wall Heating Rates and Aerodynamics on a Film-Cooled Transonic Turbine Blade", ASME *Journal of Turbomachinery*, **113**, pp. 493-501.

Coakley, T. J., 1983, "Turbulence Modeling Methods for the Compressible Navier-Stokes Equations," AIAA Paper, 83-1693, p.

Godunov, S.K., Zabrodin, A.V., Ivanov, M.Ja., Kraiko, A.N., Prokopov G.P., 1976, *Numerical Solution of gasdynamics Multidimensional Problems* (in Russian), Nauka, Moscow, p. 400.

Kapteijn, C., Amecke, J., and Michelassi, V., 1996, "Aerodynamic Performance of a Transonic Turbine Guide Vane With Trailing Edge Coolant Ejection: Part I - Experimental Approach," ASME *Journal of Turbomachinery*, **118**, pp. 519-528.

Krupa, V.G., and Ivanov, M.Ja., 1994, "Solution of Navier-Stokes Equations Using High Accuracy Monotone Schemes", AGARD Lecture Series TCP 02/LS198.

Kurmanov, B.I., and Podvidz, G.L., 2001, "The Flow Calculation in Turbine Cascades Using the Navier-Stokes Equations and q-ω Model of Turbulence" (In Russian), *Scientific Paper of TSAGI*, **3-4**, pp. 81-95.

Leylek, J.H., and Zerkle, R.D., 1994, "Discrete-Jet Film Cooling: A Comparison of Computational Results With Experiment", ASME *Journal of Turbomachinery*, **116**, pp. 358-359.

Pietrzyk, J., Bogard, D.G., and Crawford, M.E., 1989, "Hydrodynamic Measurements of Jets in Crossflow for Gas Turbine Film Cooling Applications", ASME *Journal of Turbomachinery*, **111**, pp. 139-145.

Sarkar, S., and Bose, T.K., 1996, "Numerical Analysis of Slot-Film Cooling: Effectiveness and Flow-Field", ASME *Journal of Fluids Engineering*, **118**, pp. 864-867.

Schobeiri, T., 1989, "Optimum Trailing Edge Ejection for Cooled Gas Turbine Blades", ASME *Journal of Turbomachinery*, **111**, pp. 510-514.

Sieverding, C.H., Arts, A., Denos, R., and Martelli, F., 1996, "Investigation of the Flow Field Downstream of a Turbine Trailing Edge Cooled Nozzle Guide Vane", ASME *Journal of Turbomachinery*, **118**, pp. 291-300.

Thole, K A., Gritsch, M., Schulz, A., and Wittig, S., 1997, "Effect of Crossflow at the Entrance to a Film-Cooling Hole," ASME *Journal of Fluids Engineering*, **119**, pp. 533-540.

Venediktov, V.D., Granovsky, A.V., Karelin, A.M., et al., 1990, *Atlas of the Experimental Characteristics of 2D Cooled Gas Turbine Cascades* (In Russian), CIAM, Moscow, p. 393.

Wilfert, G., and Fottner, L., 1996, "The Aerodynamic Mixing Effect of Discrete Cooling Jets With Mainstream Flow on a Highly Loaded Turbine Blade," ASME *Journal of Turbomachinery*, **118**, pp. 468-478.